

# **Studies with Improved Renormalization Group Techniques**

by

**Gregory James Petropoulos**

B.S., University of Connecticut, 2010

M.S., University of Colorado, 2013

A thesis submitted to the  
Faculty of the Graduate School of the  
University of Colorado in partial fulfillment  
of the requirements for the degree of  
Doctor of Philosophy  
Department of Physics

2014

This thesis entitled:  
Studies with Improved Renormalization Group Techniques  
written by Gregory James Petropoulos  
has been approved for the Department of Physics

---

Anna Hasenfratz

---

Prof. Thomas DeGrande

---

Prof. Ethan Neil

---

Prof. Senarath de Alwis

---

Prof. Thomas A. Manteuffel

Date \_\_\_\_\_

The final copy of this thesis has been examined by the signatories, and we find that both the content and the form meet acceptable presentation standards of scholarly work in the above mentioned discipline.

Petropoulos, Gregory James (Ph.D., Physics)

Studies with Improved Renormalization Group Techniques

Thesis directed by Prof. Anna Hasenfratz

## Dedication

To all of the fluffy kitties.

## **Acknowledgements**

Here's where you acknowledge folks who helped. But keep it short, i.e., no more than one page, as required by the Grad School Specifications.

## Contents

### Chapter

<b>1</b>	Introduction	1
1.1	Motivation . . . . .	1
1.2	Organization . . . . .	1
<b>2</b>	Strongly Coupled Physics Beyond the Standard Model	3
<b>3</b>	Lattice Field Theory	4
<b>4</b>	Monte Carlo Renormalization Group	5
4.1	Running Coupling . . . . .	5
4.2	Renormalization Group . . . . .	5
4.3	Monte Carlo Renormalization Group . . . . .	5
4.3.1	Blocking . . . . .	5
4.4	Wilson Flow . . . . .	6
4.5	Introduction and overview of methods & results . . . . .	6
4.6	Two-lattice matching procedures and the need for optimization . . . . .	8
4.6.1	Traditional MCRG . . . . .	9
4.6.2	Wilson-flowed MCRG . . . . .	9
4.7	Results . . . . .	12
4.7.1	Traditional MCRG . . . . .	12

4.7.2	Wilson-flowed MCRG . . . . .	14
4.8	Conclusions . . . . .	15
<b>5</b>	<b>Wilson Flow</b>	<b>16</b>
5.1	MCRG Results . . . . .	16
5.1.1	The Simulation . . . . .	16
5.2	Wilson Flow Results . . . . .	16
5.3	Introduction . . . . .	16
5.4	Improving gradient flow step scaling . . . . .	18
5.5	Testing improvement with 4-flavor SU(3) gauge theory . . . . .	21
5.6	Infrared fixed point in 12-flavor SU(3) gauge theory . . . . .	24
5.7	Conclusion and summary . . . . .	27
5.8	Wilson Flow MCRG Results . . . . .	30
<b>6</b>	<b>Wilson Flow MCRG</b>	<b>31</b>
6.1	MCRG Results . . . . .	31
6.1.1	The Simulation . . . . .	31
6.2	Wilson Flow Results . . . . .	31
6.3	Monte Carlo Renormalization Group . . . . .	32
6.4	Wilson-flow-optimized MCRG . . . . .	34
6.5	Results for 12 Flavors . . . . .	34
6.6	Conclusion . . . . .	35
6.7	Wilson Flow MCRG Results . . . . .	36
	<b>Bibliography</b>	<b>39</b>

## Tables

### Table



## Figures

### Figure

4.1	.....	6
4.2	Examples of two-lattice matching optimization for 12-flavor systems. Left: Optimization of the HYP-smearing parameter $\alpha$ in the RG blocking transformation, for $\beta_F = 5.0$ . Right: Optimization of the Wilson flow time $t_f$ with fixed $\alpha = 0.5$ , for $\beta_F = 4.5$ . In both cases, the uncertainties on the data points are dominated by averaging over the different observables as described in the text. ....	10
4.3	Results for the bare step-scaling function $s_b$ from traditional MCRG two-lattice matching with $24^3 \times 48$ , $12^3 \times 24$ and $6^3 \times 12$ lattice volumes, for $N_f = 8$ (left) and $N_f = 12$ (right). The blue dashed lines are perturbative predictions for asymptotically weak coupling. ....	13
4.4	Preliminary results for the bare step-scaling function $s_b$ from Wilson-flowed MCRG two-lattice matching with $24^3 \times 48$ and $12^3 \times 24$ lattice volumes, for $N_f = 8$ (left) and $N_f = 12$ (right) with fixed HYP-smearing parameters (0.5, 0.2, 0.2). The blue dashed lines are perturbative predictions for asymptotically weak coupling. ....	14
5.1	Continuum extrapolations of the discrete $\beta_{\text{lat}}$ function of the $N_f = 4$ system at $\tilde{g}_c^2(L) = 2.2$ with several different values of the $t$ -shift coefficient $\tau_0$ . The dotted lines are independent linear fits at each $\tau_0$ , which predict a consistent continuum value. .	22

5.2	Continuum extrapolations of the discrete $\beta_{\text{lat}}$ function of the $N_f = 4$ system for several different $\tilde{g}_c^2(L)$ values. For $\tilde{g}_c^2(L) = 1.8, 2.2$ and $2.6$ $\tau_0 = -0.02$ is near-optimal, while the larger couplings $\tilde{g}_c^2(L) = 3.0$ and $3.4$ require $\tau_0 = -0.01$ to remove most $\mathcal{O}(a^2)$ effects. The colored points at $(a/L)^2 = 0$ are the continuum extrapolated results, while the black crosses at $(a/L)^2 = 0$ show the corresponding two-loop perturbative predictions. . . . .	23
5.3	The $N_f = 12$ running coupling $g_c^2(L)$ versus the bare coupling $\beta_F$ on several volumes, for $c = 0.2$ . Crossings between results from different volumes predict the finite volume IRFP coupling $g_\star^2(L)$ in this scheme. . . . .	25
5.4	Continuum extrapolations of the 12-flavor finite volume IRFP $g_\star^2(L)$ , with several different $t$ -shift coefficients $\tau_0$ for fixed scale change $s = 2$ . The dotted lines are a joint linear fit constrained to have the same $(a/L)^2 = 0$ intercept, which gives $g_\star^2 = 6.21(25)$ . . . . .	28
5.5	Continuum extrapolations of the 12-flavor finite volume IRFP $g_\star^2(L)$ , with several different scale changes for the near-optimal improvement coefficient $\tau_{\text{opt}} \approx 0.04$ . The $s = 4/3$ and $3/2$ data points are horizontally displaced for greater clarity. The dashed lines are a joint linear fit constrained to have the same $(a/L)^2 = 0$ intercept, which gives $g_\star^2 = 6.18(20)$ . . . . .	29
6.1	The Wilson flow (blue) moves systems on a surface of constant lattice scale $a$ (normal to the orange renormalized trajectory) in the infinite-dimensional coupling space. Wilson-flow-optimized MCRG tunes the flow time to bring the system close to the renormalized trajectory (yellow star), so that MCRG blocking (green) quickly reaches the renormalized trajectory. . . . .	37

- 6.2 The bare step-scaling function  $s_b$  predicted by three-lattice matching with  $6^4$ ,  $12^4$  and  $24^4$  lattices blocked down to  $3^4$ , comparing three different renormalization schemes. The error bars come from the standard deviation of predictions using the different observables discussed in Section 6.3. . . . . 37
- 6.3 As in Fig. 6.2, the bare step-scaling function  $s_b$  for three different renormalization schemes from three-lattice matching, now using  $8^4$ ,  $16^4$  and  $32^4$  lattices blocked down to  $4^4$ . . . . . 38
- 6.4 The bare step-scaling function  $s_b$  for scheme 1, comparing three-lattice matching using different volumes:  $6^4$ ,  $12^4$  and  $24^4$  lattices blocked down to  $3^4$  (black  $\times$ s) as well as  $8^4$ ,  $16^4$  and  $32^4$  lattices blocked down to  $4^4$  (blue bursts) and  $2^4$  (red crosses). 38

## **Chapter 1**

### **Introduction**

#### **1.1 Motivation**

Strongly coupled quantum field theories play a vial part in our current understanding of the universe.

#### **1.2 Organization**

I grappled with how to organize this thesis for some time. I finally decided that it would be easiest for the majority of the readers as well as myself if follow the chronology of my work.

Before delving into my own work, I use chapter 2 to set the stage. In this chapter I discuss the reasons that the system I primarily study are interesting and why it is important to develop new techniques for lattice studies. I also use for In Chapter 2 I discuss the motivations that lead both to this thesis and the broader effort by the Lattice community.

Chapter 3 provides the reader with a brief overview of what goes into a lattice field theory calculation. This topic is a subject of many books, my goal is to provide the reader with a flavor of how a lattice caluclation is performed and highlight areas that are useful in later sections.

Chapter 5 puts chapter 4 into practice. I provide the details of our calculations and present our results. For consistency I discuss MCRG first followed by Wilson Flow and finally Wilson Flow MCRG.

Chapter 6

In chapter 7 I make some final remarks about interpreting our results. I will also summarize other methods that our group used to study this system. As expected all of our results show that  $SU(3)$  gauge theories with 12 chiral fermions are conformal.

## Chapter 2

### Strongly Coupled Physics Beyond the Standard Model

## Chapter 3

### Lattice Field Theory

## Chapter 4

### Monte Carlo Renormalization Group

#### 4.1 Running Coupling

#### 4.2 Renormalization Group

#### 4.3 Monte Carlo Renormalization Group

##### 4.3.1 Blocking

In a lattice simulation the quantities stored in the computer are the link variables. The link variable  $U_{n,\mu}$  encodes the gauge field at sight  $n$  in all four  $\hat{\mu}$  directions. A MCRG blocking step is a transformation that takes two links  $U_{n,\mu}$  and  $U_{n+\hat{\mu},\mu}$  and creates one link with twice the lattice spacing of the initial two links. The blocked lattice will have a factor of  $2^N$  less links than the original lattice. In four dimensions this means that an observable such as a Wilson loop will have a factor of 16 less statistics on the blocked lattice compared to the original lattice. Fortunately, on an  $N$  dimensional hyper cubic lattice there are  $2^N$  unique ways to perform this blocking. Therefore in four dimensions there are 16 unique blocking configurations. We can preserve statistics in our calculation by performing all of the unique blockings and averaging all of the observables from those blockings together. Additionally we store the blocked links on a lattice of the original cardinality using offsets as shown in 4.1.

The blocked links have a lattice spacing of twice the original lattice,  $a' = 2a$  such that the physical size of the box has not been changed.



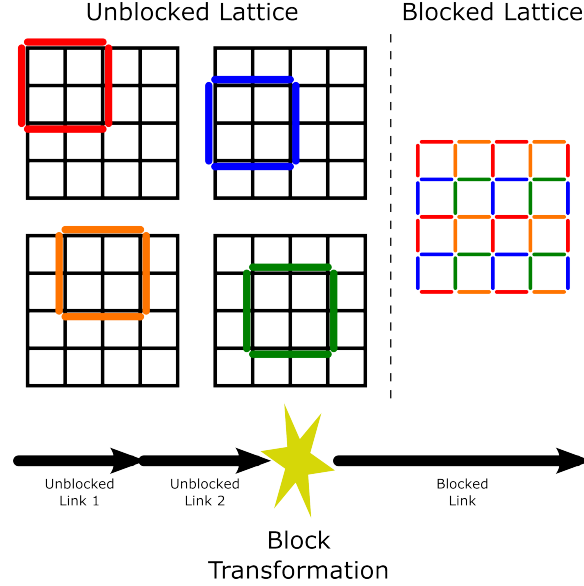


Figure 4.1:

#### 4.4 Wilson Flow

#### 4.5 Introduction and overview of methods & results

In recent years, many groups have initiated lattice investigations of strongly-coupled gauge-fermion systems beyond QCD. While the ultimate goal of these efforts is to explore potential new physics beyond the standard model, an essential step is to improve our theoretical understanding of the basic properties of these non-perturbative systems. Here we study the renormalization group properties of SU(3) gauge theories with  $N_f = 8$  and 12 nearly-massless fermions in the fundamental representation, through the Monte Carlo Renormalization Group (MCRG) two-lattice matching technique. This is one of several complementary analyses we are currently carrying out, two more of which (investigating Dirac eigenmode scaling and finite-temperature transitions) are discussed in other contributions to these proceedings [35, 52]. Recent references on SU(3) gauge theories with  $N_f = 8$  and 12 include [23, 24, 4, 21, 42]; earlier works are reviewed in Ref. [30].

In Refs. [34, 33], one of us studied MCRG two-lattice matching for the 12-flavor system with nHYP-smearred staggered actions very similar to those we use here. Our gauge action includes both fundamental and adjoint plaquette terms, with coefficients related by  $\beta_A = -0.25\beta_F$ . The

negative adjoint plaquette term lets us avoid a well-known spurious ultraviolet fixed point caused by lattice artifacts, and implies  $\beta_F = 12/g^2$  at the perturbative level. In our fermion action, we use nHYP smearing with parameters  $(0.5, 0.5, 0.4)$ , instead of the  $(0.75, 0.6, 0.3)$  used by Refs. [34, 33]. By changing the nHYP-smearing parameters in this way, we can access stronger couplings without encountering numerical problems. At such strong couplings, for both  $N_f = 8$  and  $N_f = 12$  we observe a lattice phase in which the single-site shift symmetry (“ $S^4$ ”) of the staggered action is spontaneously broken (“ $\mathcal{S}^4$ ”) [18, 52].<sup>1</sup> In this work we only investigate couplings weak enough to avoid the  $\mathcal{S}^4$  lattice phase.

In the next section, we review how the MCRG two-lattice matching technique determines the step-scaling function  $s_b$  in the bare parameter space. Although working entirely with bare parameters would be disadvantageous if our aim were to produce renormalized phenomenological predictions for comparison with experiment, our current explorations of the phase structures of the 8- and 12-flavor systems benefit from this fully non-perturbative RG approach, especially for relatively strong couplings. In Section 4.7.1 we present our results from the traditional MCRG two-lattice matching technique. While our 8-flavor  $s_b$  is significantly different from zero, for  $N_f = 12$  we observe  $s_b \lesssim 0$  for  $\beta_F < 8$ , indicating an infrared fixed point (IRFP).

We emphasize that while the existence of an IRFP is physical (scheme-independent), the coupling at which it is located depends on the choice of renormalization scheme. A limitation of traditional MCRG two-lattice matching is the need to optimize the RG blocking transformation separately for each lattice coupling  $\beta_F$ . As we explain below, this optimization forces us to probe a different renormalization scheme for each  $\beta_F$ , so that the bare step-scaling function we obtain is a composite of many different discrete  $\beta$  functions.

To address this issue, in Section 4.6.2 we propose a new, improved procedure that predicts a bare step-scaling function corresponding to a unique  $\beta$  function. This improved procedure applies the Wilson flow [46, 43] to the lattice system before performing the RG blocking transformation. Because the Wilson flow moves the system in the infinite-dimensional space of lattice-action terms

---

<sup>1</sup> Ref. [21] recently interpreted the  $\mathcal{S}^4$  lattice phase in terms of relevant next-to-nearest neighbor interactions.

without changing the lattice scale, we can use it to approach the renormalized trajectory corresponding to a fixed RG blocking transformation. By optimizing the flow time  $t_f$  at each coupling, all with the same renormalization scheme, we can carry out the two-lattice matching without a need for further optimization. We present some promising but preliminary results of this approach in Section 4.7.2.

#### 4.6 Two-lattice matching procedures and the need for optimization

Two-lattice matching is most easily described in the context of confining systems, where it locates pairs of couplings  $(\beta_F, \beta'_F)$  for which lattice correlation lengths obey  $\xi(\beta_F) = 2\xi(\beta'_F)$ . We proceed by repeatedly applying RG blocking transformations (with scale factor  $s = 2$ ) to lattices of volume  $24^3 \times 48$ ,  $12^3 \times 24$  and  $6^3 \times 12$ .<sup>2</sup> Under RG blocking on the  $m = 0$  critical surface, the system flows toward the renormalized trajectory in irrelevant directions, and along it in the relevant direction. By blocking the larger lattices (with  $\beta_F$ )  $n_b$  times and the smaller lattices (with  $\beta'_F$ ) only  $n_b - 1$  times, we obtain blocked systems with the same lattice volume. If these blocked systems have both flowed to the same point on the renormalized trajectory, then we can conclude that  $\xi(\beta_F) = 2\xi(\beta'_F)$  on the unblocked systems, as desired.

We determine whether the blocked systems have flowed to the same point on the renormalized trajectory by matching several short-range gauge observables: the plaquette, all three six-link loops, and two planar eight-link loops. For a given  $\beta_F$ , each observable may predict a different  $\Delta\beta_F \equiv \beta_F - \beta'_F$ . The spread in these results is a systematic error that dominates our uncertainties.

In an IR-conformal system, the gauge coupling that is relevant at the perturbative gaussian FP becomes irrelevant at the IRFP. The renormalized trajectory connects these two fixed points. When RG flows approach this renormalized trajectory, the two-lattice matching can be performed and interpreted the same way as in confining systems. In this region the gauge coupling flows to stronger couplings,  $\Delta\beta_F > 0$  corresponding to a negative RG  $\beta$  function. The situation is less clear at stronger couplings where we might naïvely expect backward flow. If there is no ultraviolet FP

---

<sup>2</sup> We are currently generating larger lattices up to  $32^3 \times 64$ , which will permit additional consistency checks.

in this region to drive the RG flow along a renormalized trajectory, the two-lattice matching might become meaningless. This issue affects every method that attempts to determine the flow of the gauge coupling in IR-conformal systems at strong coupling. In all published studies that report an IRFP, backward flow has only been observed in a very limited range of couplings in the immediate vicinity of the IRFP (cf. Ref. [30]).

Since we can block our lattices only a few times, we must optimize the two-lattice matching by requiring that consecutive RG blocking steps yield the same  $\Delta\beta_F$ . We identify the optimized  $\Delta\beta_F$  with the bare step-scaling function  $s_b$ . In the following subsections, we describe two different ways to perform this optimization. The traditional technique optimizes the RG blocking transformation (renormalization scheme). The new method we propose in Section 4.6.2 instead applies the Wilson flow to the lattice system prior to RG blocking, and optimizes the flow time  $t_f$ .

#### 4.6.1 Traditional MCRG

As in Refs. [34, 33], we use RG blocking transformations that include two sequential HYP smearings with parameters  $(\alpha, 0.2, 0.2)$ , and optimize  $\alpha$  as shown in the left panel of Fig. 4.2. Qualitatively, this optimization finds the renormalization scheme for which the renormalized trajectory passes as close as possible to the lattice system with coupling  $\beta_F$ . Without optimization, residual flows in irrelevant directions can distort the results: this is the reason  $\Delta\beta_F$  changes with  $\alpha$  in Fig. 4.2, and also explains why increasing the number of blocking steps reduces this  $\alpha$ -dependence.

The downside of optimizing the RG blocking transformation in this manner is that we have to use a different renormalization scheme for each  $\beta_F$ . As a result, the bare step-scaling function we obtain is a composite of many different discrete  $\beta$  functions.

#### 4.6.2 Wilson-flowed MCRG

As an alternative to optimizing the RG blocking transformation, and thus changing the renormalization scheme at each coupling  $\beta_F$ , here we propose to use the Wilson flow to move the lattice system as close as possible to the renormalized trajectory of a fixed renormalization scheme.

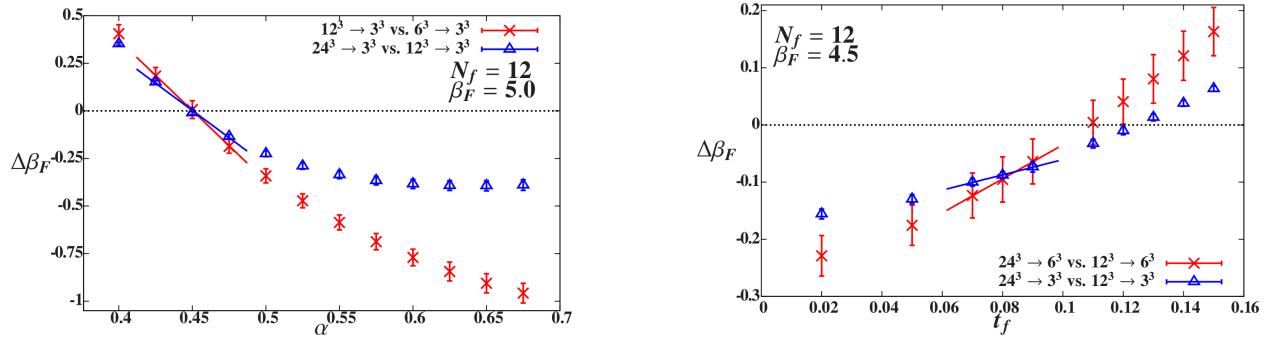


Figure 4.2: Examples of two-lattice matching optimization for 12-flavor systems. Left: Optimization of the HYP-smearing parameter  $\alpha$  in the RG blocking transformation, for  $\beta_F = 5.0$ . Right: Optimization of the Wilson flow time  $t_f$  with fixed  $\alpha = 0.5$ , for  $\beta_F = 4.5$ . In both cases, the uncertainties on the data points are dominated by averaging over the different observables as described in the text.

The Wilson flow is a continuous smearing transformation [46] that can be related to the  $\overline{\text{MS}}$  running coupling in perturbation theory [43]. Refs. [26, 27] recently used the Wilson flow to compute a renormalized step-scaling function in a way similar to Schrödinger functional methods. While this approach appears very promising, it is based on perturbative relations that are only fully reliable at weak coupling. Here we do not use this perturbative connection, instead applying the Wilson flow as a continuous smearing that removes UV fluctuations. The Wilson flow moves the system along a surface of constant lattice scale in the infinite-dimensional action-space; it is not a renormalization group transformation and does not change the IR properties of the system.

Our goal is to use a one-parameter Wilson flow transformation to move the lattice system as close as possible to the renormalized trajectory of our fixed RG blocking transformation. We proceed by carrying out two-lattice matching after applying the Wilson flow for a flow time  $t_f$  on all lattice volumes. (The Wilson flow is run only on the unblocked lattices, not in between RG blocking steps.) As above, since we can block our lattices only a few times, we must optimize  $t_f$  by requiring that consecutive RG blocking steps yield the same  $\Delta\beta_F$ , as shown in the right panel of Fig. 4.2. As for traditional MCRG, increasing the number of blocking steps reduces the dependence on the optimization parameter; in the limit  $n_b \rightarrow \infty$ , our results would be independent of  $t_f$ .

With Wilson-flowed MCRG we can efficiently determine bare step-scaling functions that correspond to unique RG  $\beta$  functions. This new capability opens up interesting directions for future studies. By comparing different  $\beta$  functions around the perturbative gaussian FP, we can study scaling violations in the lattice system. In IR-conformal systems, we can investigate the scheme-dependence of the  $\beta$  function near the IRFP, an issue explored in perturbation theory by Ref. [51].

## 4.7 Results

### 4.7.1 Traditional MCRG

Our results for the bare step-scaling function  $s_b$  from traditional MCRG two-lattice matching are shown in Fig. 4.3. On the largest  $24^3 \times 48$  lattices that we use in this current study, we work with fermion masses  $m = 0.0025$  to stay near the  $m = 0$  critical surface. Under RG blocking with scale factor  $s$ , the fermion mass changes as  $s^{1+\gamma_m}$  where  $\gamma_m$  is the mass anomalous dimension. Therefore we use  $m = 0.01$  on  $12^3 \times 24$  and  $m = 0.02$  on  $6^3 \times 12$  lattices. We have explicitly checked that these masses are small enough to introduce only negligible finite-mass effects, by generating lattices with  $m = 0$  for some points and obtaining indistinguishable results.

While our 8-flavor results for  $s_b$  are significantly different from zero for all couplings we can explore, for  $N_f = 12$  we find  $s_b \lesssim 0$  for  $\beta_F < 8$ , indicating an IRFP. Recall that our optimization of the RG blocking transformation means that we use a different renormalization scheme for each coupling  $\beta_F$ , so these bare step scaling functions are composites of several different discrete  $\beta$  functions. For example, with  $N_f = 12$  at  $5 \leq \beta_F \leq 6$ , our optimization selects renormalization schemes with the fixed point near  $\beta_F$ , so that  $s_b$  is roughly consistent with zero over an extended range. Both our  $N_f = 8$  and 12 simulations encounter the  $\mathcal{S}^4$  lattice phase at strong coupling, where we cannot perform matching. As in Refs. [34, 33], we do not explore weak enough couplings to recover the two-loop perturbative predictions  $s_b \approx 0.6$  (0.3) for  $N_f = 8$  (12).

As mentioned above, the error bars shown in Fig. 4.3 are dominated by the spread in results from matching four-, six- and eight-link loops. Each of these observables can predict a different optimal  $\alpha$ , and for fixed  $\alpha$  each can predict a different  $\Delta\beta_F$ . Preliminary results presented at the conference determined uncertainties from the full spread of optimal  $\alpha$  predicted by the different observables. Here, instead, we average  $\Delta\beta_F$  for the different observables at fixed  $\alpha$ , and use these combined data to optimize  $\alpha$  and find the associated uncertainties.

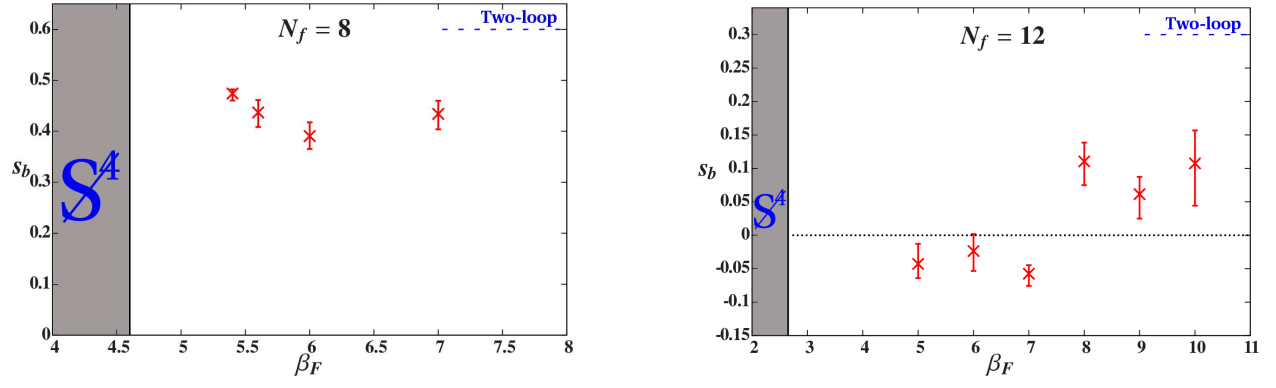


Figure 4.3: Results for the bare step-scaling function  $s_b$  from traditional MCRG two-lattice matching with  $24^3 \times 48$ ,  $12^3 \times 24$  and  $6^3 \times 12$  lattice volumes, for  $N_f = 8$  (left) and  $N_f = 12$  (right). The blue dashed lines are perturbative predictions for asymptotically weak coupling.



#### 4.7.2 Wilson-flowed MCRG

Fig. 4.4 presents our results for the bare step-scaling function  $s_b$  from Wilson-flowed MCRG two-lattice matching. We continue using two sequential HYP smearings in our RG blocking transformation, but now fix the smearing parameters to  $(0.5, 0.2, 0.2)$ . We again use  $24^3 \times 48$  and  $12^3 \times 24$  lattices with fermion masses  $m = 0.0025$  and  $m = 0.01$ , respectively, and determine uncertainties in the same way as described in the previous subsection. In this preliminary study we don't yet employ the volume-corrected optimization discussed in Ref. [34]; for our lattice volumes, Ref. [34] found that neglecting this finite-volume correction introduces only a small additional error. Our final results will use the appropriate optimization, and will also present further consistency checks from larger lattices up to  $32^3 \times 64$ .

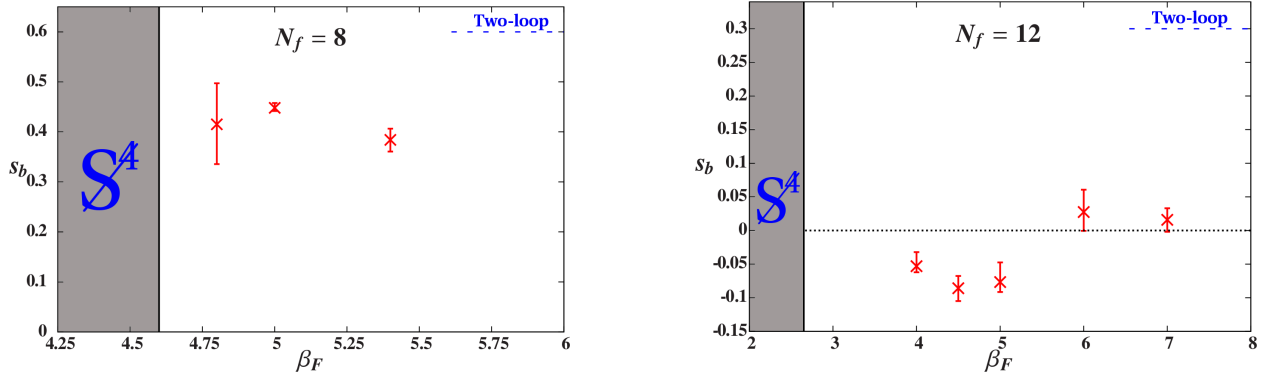


Figure 4.4: Preliminary results for the bare step-scaling function  $s_b$  from Wilson-flowed MCRG two-lattice matching with  $24^3 \times 48$  and  $12^3 \times 24$  lattice volumes, for  $N_f = 8$  (left) and  $N_f = 12$  (right) with fixed HYP-smearing parameters  $(0.5, 0.2, 0.2)$ . The blue dashed lines are perturbative predictions for asymptotically weak coupling.

While our results in Fig. 4.4 from combining the Wilson flow with MCRG two-lattice matching are qualitatively similar to the results of the traditional approach in Fig. 4.3, we can now identify the bare step-scaling function  $s_b$  with a unique discrete  $\beta$  function. In the renormalization scheme defined by our RG blocking transformation with HYP-smearing parameters  $(0.5, 0.2, 0.2)$ , we find a 12-flavor IRFP at  $5 < \beta_F^* \lesssim 6$ . Although  $\beta_F^*$  is scheme-dependent, the existence of this IRFP is physical. We are currently exploring other choices of renormalization schemes, to non-

perturbatively investigate the scheme-dependence of the  $\beta$  function near the IRFP [51]. At weaker couplings, we will also attempt to use similar explorations to study scaling violations in our lattice systems.

## 4.8 Conclusions

We have proposed a new, improved MCRG two-lattice matching procedure that uses the Wilson flow to eliminate the need for optimization of the RG blocking transformation. Both traditional MCRG and Wilson-flowed MCRG produce bare step scaling functions  $s_b$  that indicate an infrared fixed point for SU(3) gauge theory with  $N_f = 12$  fundamental fermions, while  $s_b$  for  $N_f = 8$  is significantly different from zero in the accessible range of lattice couplings. The results obtained by combining the Wilson flow with two-lattice matching correspond to a unique  $\beta$  function, unlike  $s_b$  from traditional MCRG, which is a composite of many different discrete  $\beta$  functions.

## Chapter 5

### Wilson Flow

#### 5.1 MCRG Results

The renormalization group has been used to study the  $SU(3)$   $N_f = 12$  system already [cite anna]. These results show that the theory is clearly conformal. The action used in these simulations is ... As part of a greater effort to study this system further we changed our action to reach stronger coupling. In this section I will present our results using MCRG with the changed action.

##### 5.1.1 The Simulation

To achieve stronger coupling we use a different lattice action. This action has [details about action]

#### 5.2 Wilson Flow Results

#### 5.3 Introduction

Asymptotically-free  $SU(N)$  gauge theories coupled to  $N_f$  massless fundamental fermions are conformal in the infrared if  $N_f$  is sufficiently large,  $N_f \geq N_f^{(c)}$ . Their renormalization group (RG)  $\beta$  functions possess a non-trivial infrared fixed point (IRFP) where the gauge coupling is an irrelevant operator. Although this IRFP can be studied perturbatively for large  $N_f$  near the value at which asymptotic freedom is lost [13, 11], as  $N_f$  decreases the fixed point becomes strongly coupled. Systems around  $N_f \approx N_f^{(c)}$  are particularly interesting strongly-coupled quantum field theories,

with non-perturbative conformal or near-conformal dynamics. Their most exciting phenomenological application is the possibility of a light composite Higgs boson from dynamical electroweak symmetry breaking [25, 45, 6, 28, 1]. Due to the strongly-coupled nature of these systems, lattice gauge theory calculations are a crucial non-perturbative tool with which to investigate them from first principles. Many lattice studies of potentially IR-conformal theories have been carried out in recent years (cf. the recent reviews [47, 31] and references therein). While direct analysis of the RG  $\beta$  function may appear an obvious way to determine whether or not a given system flows to a conformal fixed point in the infrared, in practice this is a difficult question to address with lattice techniques. In particular, extrapolation to the infinite-volume continuum limit is an essential part of such calculations.

In the case of SU(3) gauge theory with  $N_f = 12$  fundamental fermions, several lattice groups have investigated the step scaling function, the discretized form of the  $\beta$  function. To date, these studies either did not reach a definite conclusion [32, 42] or may be criticized for not properly taking the infinite-volume continuum limit [7, 8, 32, 34, 40, 50]. At the same time, complementary numerical investigations have been carried out, considering for example the spectrum, or bulk and finite-temperature phase transitions [20, 22, 5, 19, 18, 16, 23, 24, 4, 3, 41]. The different groups performing these studies have not yet reached consensus regarding the infrared behavior of the 12-flavor system.

Our own  $N_f = 12$  results favor the existence of a conformal IRFP, which we observe in Monte Carlo RG studies [34, 50]. Our zero- and finite-temperature studies of the lattice phase diagram show a bulk transition consistent with conformal dynamics [52, 36]. From the Dirac eigenvalue spectrum [16], and from finite-size scaling of mesonic observables [14], we obtain consistent predictions for a relatively small fermion mass anomalous dimension:  $\gamma_m^* = 0.32(3)$  and  $0.235(15)$ , respectively. While this conclusion, if correct, would render the 12-flavor system unsuitable for composite Higgs phenomenology, we consider  $N_f = 12$  to remain an important case to study. Considerable time and effort has already been invested to obtain high-quality lattice data for the 12-flavor system. Until different methods of analyzing and interpreting these data can be reconciled – or the causes of any

remaining disagreements can be clarified – it will not be clear which approaches are most reliable and most efficient to use in other contexts.

The recent development of new running coupling schemes based on the gradient flow [44, 43, 26, 27, 29] provides a promising opportunity to make progress. In this work we investigate step scaling using the gradient flow running coupling.<sup>1</sup> We begin by introducing a non-perturbative improvement to this technique, which increases our control over the continuum extrapolation by reducing the leading-order cut-off effects. While this improvement is phenomenological in the sense that we have not derived it systematically through a full improvement program, it is generally applicable to any lattice gauge theory of interest and can remove all  $\mathcal{O}(a^2)$  cut-off effects. We illustrate it first for 4-flavor SU(3) gauge theory, a system where the running coupling has previously been studied with both Wilson [54] and staggered [48, 26, 27] fermions. We then turn to  $N_f = 12$ , where we show that the infinite-volume continuum limit is well defined and predicts an IRFP. In both the 4- and 12-flavor systems, our improvement can remove all observable  $\mathcal{O}(a^2)$  effects, despite the dramatically different IR dynamics. We conclude with some comments on other systems where improved gradient flow step scaling may profitably be applied.

## 5.4 Improving gradient flow step scaling

The gradient flow is a continuous invertible smearing transformation that systematically removes short-distance lattice cut-off effects [44, 43]. At flow time  $t = a^2 t_{\text{lat}}$  it can be used to define a renormalized coupling at scale  $\mu = 1/\sqrt{8t}$

$$g_{\text{GF}}^2(\mu = 1/\sqrt{8t}) = \frac{1}{\mathcal{N}} \langle t^2 E(t) \rangle, \quad (5.1)$$

where “ $a$ ” is the lattice spacing,  $t_{\text{lat}}$  is dimensionless, and the energy density  $E(t) = -\frac{1}{2} \text{ReTr} [G_{\mu\nu}(t) G^{\mu\nu}(t)]$  is calculated at flow time  $t$  with an appropriate lattice operator. We evolve the gradient flow with the Wilson plaquette term and use the usual “clover” or “symmetric” definition of  $G_{\mu\nu}(t)$ . The normalization  $\mathcal{N}$  is set such that  $g_{\text{GF}}^2(\mu)$  agrees with the continuum  $\overline{\text{MS}}$  coupling at tree level.

---

<sup>1</sup> We are aware of two other ongoing investigations of the  $N_f = 12$  gradient flow step scaling function, by the authors of Ref. [26] and Ref. [42].

If the flow time is fixed relative to the lattice size,  $\sqrt{8t} = cL$  with  $c$  constant, the scale of the corresponding coupling  $g_c^2(L)$  is set by the lattice size. Like the well-known Schrödinger functional (SF) coupling,  $g_c^2(L)$  can be used to compute a step scaling function [26, 27, 29]. The greater flexibility of the gradient flow running coupling is a significant advantage over the more traditional SF coupling. A single measurement of the gradient flow will provide  $g_c^2$  for a range of  $c$ . In our study we obtain  $g_c^2$  for all  $0 \leq c \leq 0.5$  separated by  $\delta t_{\text{lat}} = 0.01$ . Each choice of  $c$  corresponds to a different renormalization scheme, which can be explored simultaneously on the same set of configurations [29].

The normalization factor  $\mathcal{N}$  in finite volume has been calculated for anti-periodic boundary conditions (BCs) in refs. [26, 27], and for SF BCs in Ref. [29]. In this work we use anti-periodic BCs, for which

$$\frac{1}{\mathcal{N}} = \frac{128\pi^2}{3(N^2 - 1)(1 + \delta(c))} \quad \delta(c) = \vartheta^4\left(e^{-1/c^2}\right) - 1 - \frac{c^4\pi^2}{3}, \quad (5.2)$$

where  $\vartheta(x) = \sum_{n=-\infty}^{\infty} x^{n^2}$  is the Jacobi elliptic function. For  $0 \leq c \leq 0.3$  the finite-volume correction  $\delta(c)$  computed in Ref. [26] is small,  $|\delta(c)| \leq 0.03$ . As explained in refs. [26, 27], the RG  $\beta$  function of  $g_{\text{GF}}^2$  is two-loop universal with SF BCs, but only one-loop universal with anti-periodic BCs.

At non-zero lattice spacing  $g_{\text{GF}}^2$  has cut-off corrections. These corrections could be  $\mathcal{O}(a)$  for unimproved actions, and even  $\mathcal{O}(a)$ -improved actions could have large  $\mathcal{O}(a^2[\log a]^n)$ -type corrections [9, 10]. In existing numerical studies of staggered or  $\mathcal{O}(a)$ -improved Wilson fermions the leading lattice corrections appear to be  $\mathcal{O}(a^2)$  [29, 53],

$$g_{\text{GF}}^2(\mu; a) = g_{\text{GF}}^2(\mu; a = 0) + a^2\mathcal{C} + \mathcal{O}(a^4[\log a]^n, a^4). \quad (5.3)$$

It is possible to remove, or at least greatly reduce, the  $\mathcal{O}(a^2)$  corrections in eq. 5.3 by defining

$$\tilde{g}_{\text{GF}}^2(\mu; a) = \frac{1}{\mathcal{N}} \langle t^2 E(t + \tau_0 a^2) \rangle, \quad (5.4)$$

where  $\tau_0 \ll t/a^2$  is a small shift in the flow time. In the continuum limit  $\tau_0 a^2 \rightarrow 0$  and  $\tilde{g}_{\text{GF}}^2(\mu) = g_{\text{GF}}^2(\mu)$ .

There are several possible interpretations of the  $t$ -shift in eq. 5.4. The gradient flow is an invertible smearing transformation, so one can consider  $\tau_0$  as an initial flow that does not change the IR properties of the system but leads to a new action. The gradient flow coupling  $\tilde{g}_{\text{GF}}^2$  in eq. 5.4 is calculated for this new action. Alternatively one can consider the replacement of  $\langle t^2 E(t) \rangle$  with  $\langle t^2 E(t + \tau_0 a^2) \rangle$  as an improved operator for the energy density. In either case the  $t$ -shift changes the  $\mathcal{O}(a^2)$  term of  $g_{\text{GF}}^2(\mu; a)$ . If we expand  $\tilde{g}_{\text{GF}}^2(\mu)$  in  $\tau_0 a^2$ ,

$$\tilde{g}_{\text{GF}}^2(\mu; a) = \frac{1}{\mathcal{N}} \langle t^2 E(t) \rangle + \frac{a^2 \tau_0}{\mathcal{N}} \left\langle t^2 \frac{\partial E(t)}{\partial t} \right\rangle, \quad (5.5)$$

and choose  $\tau_0$  such that the second term in eq. 5.5 cancels the  $a^2 \mathcal{C}$  term in eq. 5.3, we remove the leading lattice artifacts

$$\tilde{g}_{\text{opt}}^2(\mu; a) = g_{\text{GF}}^2(\mu; a = 0) + \mathcal{O}(a^4 [\log a]^n, a^4). \quad (5.6)$$

Full  $\mathcal{O}(a^2)$  improvement through a systematic improvement program would require adding terms to improve the flow equation, the action, the boundary conditions, and the energy density operator  $\langle t^2 E(t) \rangle$  [53]. Since our proposed improvement involves only a single parameter  $\tau_0$ , this  $\tau_0$  itself must depend on other parameters, most importantly on  $\tilde{g}_{\text{GF}}^2(\mu)$  and on the bare coupling through the lattice spacing dependence of the term  $\left\langle t^2 \frac{\partial E(t)}{\partial t} \right\rangle$  in eq. 5.5. Optimizing  $\tau_0$  both in the renormalized and bare couplings could remove the predictive power of the method. Fortunately, as we will see in the next section, our numerical tests indicate that it is sufficient to choose  $\tau_0$  to be a constant or only weakly  $\tilde{g}_{\text{GF}}^2(\mu)$  dependent to remove most  $\mathcal{O}(a^2)$  lattice artifacts.

Since the gradient flow is evaluated through numerical integration, the replacement  $g_{\text{GF}}^2 \rightarrow \tilde{g}_{\text{GF}}^2$  can be done by a simple shift of  $t$  without incurring any additional computational cost. The optimal  $t$ -shift  $\tau_{\text{opt}}$  can be identified by a simple procedure when the gradient flow is used for scale setting, which we will consider in a future publication. In this paper we concentrate on the step scaling function and find the  $\tau_{\text{opt}}$  that removes the  $\mathcal{O}(a^2)$  terms of the discrete  $\beta$  function corresponding to scale change  $s$ ,

$$\beta_{\text{lat}}(g_c^2; s; a) = \frac{\tilde{g}_c^2(L; a) - \tilde{g}_c^2(sL; a)}{\log(s^2)}. \quad (5.7)$$

## 5.5 Testing improvement with 4-flavor SU(3) gauge theory

We illustrate the  $t$ -shift improvement with the  $N_f = 4$  SU(3) system. This theory was recently studied by refs. [26, 27] using gradient flow step scaling with staggered fermions. The 4-flavor SF running coupling was previously considered in Ref. [54] using  $\mathcal{O}(a)$ -improved Wilson fermions, and in Ref. [48] using staggered fermions. In our calculations we use nHYP-smeared [39, 38] staggered fermions and a gauge action that includes an adjoint plaquette term in order to move farther away from a well-known spurious fixed point in the adjoint–fundamental plaquette plane [18]. As in Ref. [26] we impose anti-periodic BCs in all four directions, which allows us to carry out computations with exactly vanishing fermion mass,  $m = 0$ . For the discrete  $\beta$  function we consider the scale change  $s = 3/2$  and compare lattice volumes  $12^4 \rightarrow 18^4$ ,  $16^4 \rightarrow 24^4$  and  $20^4 \rightarrow 30^4$ . We accumulated 500–600 measurements of the gradient flow coupling, with each measurement separated by 10 molecular dynamics time units (MDTU), at 7–8 values of the bare gauge coupling on each volume. We consider the  $c = 0.25$  scheme, as opposed to  $c = 0.3$  used in Ref. [26], because smaller  $c$  gives better statistics at the expense of larger lattice artifacts. As discussed above, we aim to reduce these lattice artifacts through the non-perturbative improvement we have introduced. We follow the fitting procedure described in Ref. [54].

Full details of this study will be presented in Ref. [15]. Here we provide a representative illustration of the  $t$ -shift optimization. Figure 5.1 shows the dependence of the discrete  $\beta$  function on  $(a/L)^2$  when  $\tilde{g}_c^2(L) = 2.2$  with several values of the  $t$ -shift parameter  $\tau_0$ . The red triangles correspond to no improvement,  $\tau_0 = 0$ . The data are consistent with linear dependence on  $a^2$  and extrapolate to 0.262(17), about  $2\sigma$  below the two-loop perturbative value of 0.301. The slope of the extrapolation is already rather small,  $b = 11(3)$ . By adding a small shift this slope can be increased or decreased. With  $\tau_0 = -0.02$  no  $\mathcal{O}(a^2)$  effects can be observed – the corresponding slope is  $b = 1.5(3.1)$  – and we identify this value as near the optimal  $\tau_{\text{opt}}$ . The data at different  $\tau_0$  extrapolate to the same continuum value, even when the slope  $b$  is larger than that for  $\tau_0 = 0$ . This is consistent with the expectation that the  $t$ -shift changes the  $\mathcal{O}(a^2)$  behavior of the system but



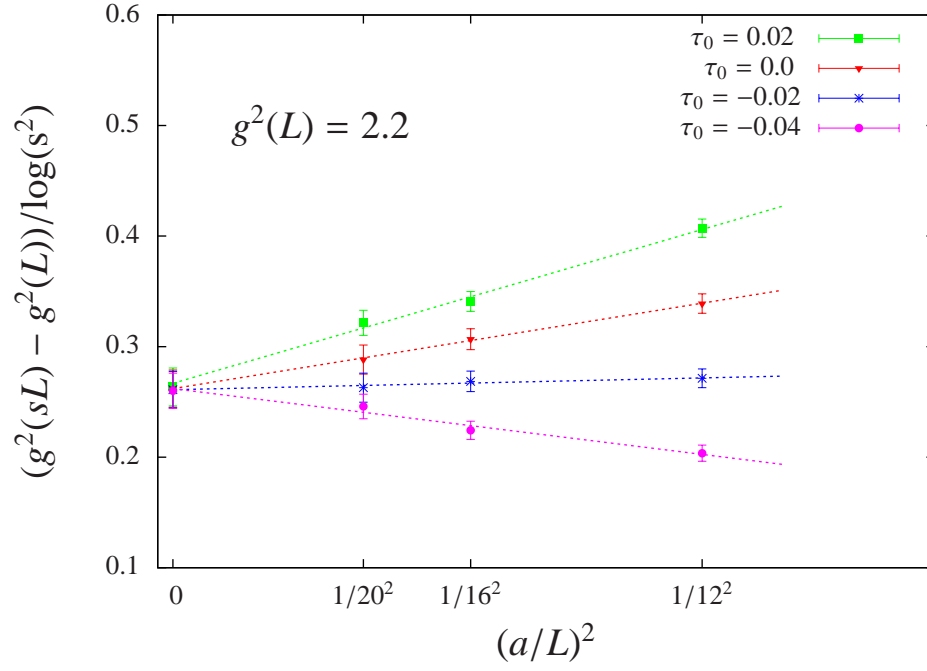


Figure 5.1: Continuum extrapolations of the discrete  $\beta_{\text{lat}}$  function of the  $N_f = 4$  system at  $\tilde{g}_c^2(L) = 2.2$  with several different values of the  $t$ -shift coefficient  $\tau_0$ . The dotted lines are independent linear fits at each  $\tau_0$ , which predict a consistent continuum value.

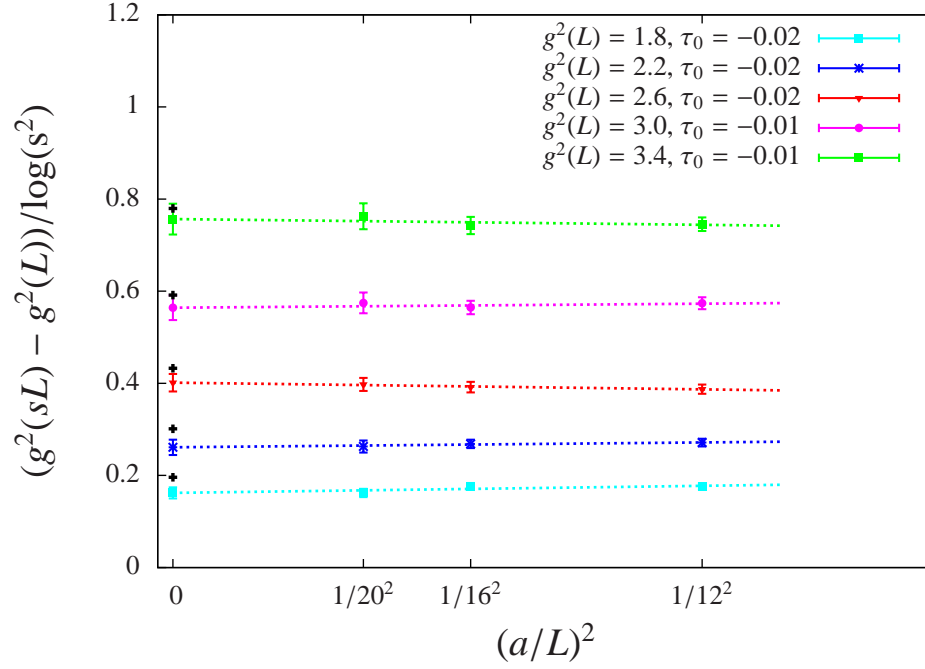


Figure 5.2: Continuum extrapolations of the discrete  $\beta_{\text{lat}}$  function of the  $N_f = 4$  system for several different  $\tilde{g}_c^2(L)$  values. For  $\tilde{g}_c^2(L) = 1.8, 2.2$  and  $2.6$   $\tau_0 = -0.02$  is near-optimal, while the larger couplings  $\tilde{g}_c^2(L) = 3.0$  and  $3.4$  require  $\tau_0 = -0.01$  to remove most  $\mathcal{O}(a^2)$  effects. The colored points at  $(a/L)^2 = 0$  are the continuum extrapolated results, while the black crosses at  $(a/L)^2 = 0$  show the corresponding two-loop perturbative predictions.

does not affect the continuum limit. Since our action produces relatively small  $\mathcal{O}(a^2)$  corrections even without improvement, the  $t$ -shift optimization has little effect on the continuum extrapolation, though the consistency between different values of  $\tau_0$  is reassuring.

It is interesting that the cut-off effects in our unimproved results, characterized by the slope  $b$  of the red triangles in Fig. 5.1, are more than three times smaller than those shown in fig. 4 of Ref. [26]. This difference grows to about a factor of four when we consider the larger  $c = 0.3$  used in that study, suggesting that the  $t$ -shift optimization could have a more pronounced effect with the action used in Ref. [26]. The cause of the reduced lattice artifacts with our action is not obvious. Both our action and that used by Ref. [26] are based on smeared staggered fermions, though we use different smearing schemes. The different smearing might have an effect, as might the inclusion of the adjoint plaquette term in our gauge action. This question is worth investigating in the future.

In principle  $\tau_{\text{opt}}$  could be different at different  $g_c^2$  couplings but in practice we found little variation. Figure 5.2 shows near-optimal continuum extrapolations of the discrete  $\beta$  function at several values of  $\tilde{g}_c^2(L)$ . At each  $\tilde{g}_c^2(L)$  the continuum extrapolated result is consistent within  $\sim 2\sigma$  with the two-loop perturbative prediction, denoted by a black cross in Fig. 5.2. Comparable consistency with perturbation theory was found in previous studies [54, 48, 26, 27].

## 5.6 Infrared fixed point in 12-flavor SU(3) gauge theory

We use the same lattice action with  $N_f = 12$  as with  $N_f = 4$  and consider six different volumes:  $12^4$ ,  $16^4$ ,  $18^4$ ,  $24^4$ ,  $32^4$  and  $36^4$ . This range of volumes allows us to carry out step scaling analyses with scale changes  $s = 4/3$ ,  $3/2$  and  $2$ . As for  $N_f = 4$  we performed simulations in the  $m = 0$  chiral limit with anti-periodic BCs in all four directions. Depending on the volume and bare coupling  $\beta_F$  we accumulated 300–1000 measurements of the gradient flow coupling  $g_c^2$  for  $0 \leq c \leq 0.5$ , with 10 MDTU separating subsequent measurements. Here we will consider only  $c = 0.2$ . Full details of our ensembles and measurements, studies of their auto-correlations, and additional analyses for  $c = 0.25$  and  $0.3$  will appear in Ref. [15]. The choice of  $c = 0.2$  minimizes the statistical errors, and we find the IRFP in this scheme to be at a weaker coupling than for larger  $c$ ,

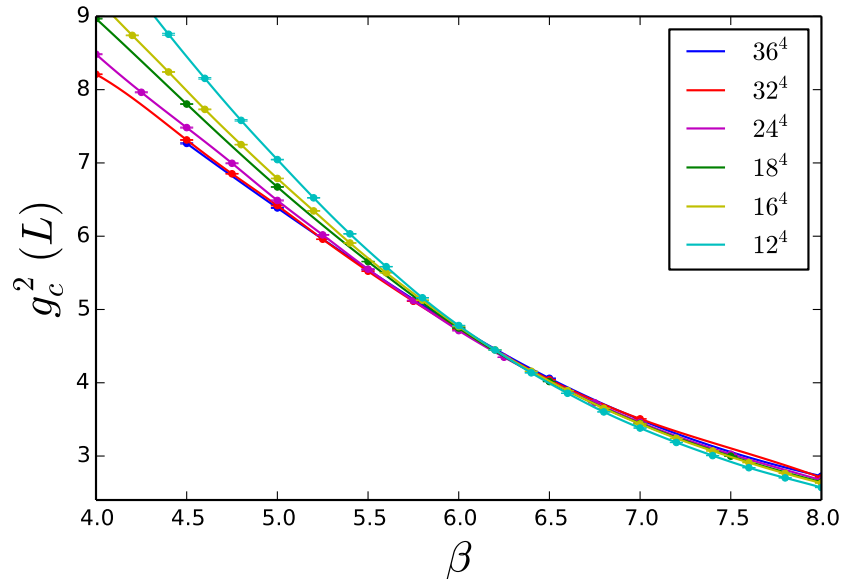


Figure 5.3: The  $N_f = 12$  running coupling  $g_c^2(L)$  versus the bare coupling  $\beta_F$  on several volumes, for  $c = 0.2$ . Crossings between results from different volumes predict the finite volume IRFP coupling  $g_*^2(L)$  in this scheme.

which is numerically easier to reach. The typical trade-off for these smaller statistical errors would be larger cut-off effects, but as discussed in previous sections these cut-off effects can be reduced by our non-perturbative improvement.

Figure 5.3 shows the running coupling  $g_c^2(L)$  as the function of the bare gauge coupling  $\beta_F$  for different volumes. The interpolating curves are from fits similar to those in Ref. [54]. The curves from different volumes cross in the range  $6.0 \leq \beta_F \leq 6.5$ . The crossing from lattices with linear size  $L$  and  $sL$  defines the finite-volume IRFP coupling  $g_\star^2(L; s)$ :

$$g_c^2(L) = g_c^2(sL) \implies g_\star^2(L; s) = g_c^2(L). \quad (5.8)$$

If the IRFP exists in the continuum limit then the extrapolation

$$\lim_{(a/L)^2 \rightarrow 0} g_\star^2(L; s) \equiv g_\star^2 \quad (5.9)$$

has to be finite and independent of  $s$ .<sup>2</sup> Figure 5.4 illustrates the continuum extrapolation of  $g_\star^2(L)$  with scale change  $s = 2$  for various choices of the  $t$ -shift parameter  $\tau_0$ . The red triangles correspond to no shift,  $\tau_0 = 0$ . Their  $(a/L)^2 \rightarrow 0$  continuum extrapolation has a negative slope, and the leading lattice cut-off effects are removed with a positive  $t$ -shift,  $\tau_{\text{opt}} \approx 0.04$ . A joint linear extrapolation of the  $\tau_0 = 0, 0.02, 0.04$  and  $0.06$  results, constrained to have the same continuum limit at  $(a/L)^2 = 0$ , predicts  $g_\star^2 = 6.21(25)$ . However, these results all come from the same measurements, and are therefore quite correlated. While it is an important consistency check that the continuum limit does not change with  $\tau_{\text{opt}}$ , just as for  $N_f = 4$ , the uncertainty in the continuum-extrapolated  $g_\star^2$  from this joint fit is not reliable.

Instead, we should consider only the results with the near-optimal  $\tau_{\text{opt}} \approx 0.04$ . As we show in Fig. 5.5,  $\tau_{\text{opt}} \approx 0.04$  is also near-optimal for scale changes  $s = 3/2$  and  $4/3$ . None of these results have any observable  $\mathcal{O}(a^2)$  effect, making the extrapolation to the continuum very stable. Each scale change predicts a continuum IRFP for  $N_f = 12$ . The three sets of results in Fig. 5.5 come from matching different volumes, making a joint fit legitimate. This continuum extrapolation

---

<sup>2</sup> We thank D. N6gr6di for useful discussions of the continuum limit.

predicts that the IR fixed point is located at renormalized coupling  $g_\star^2 = 6.18(20)$  in the  $c = 0.2$  scheme.

## 5.7 Conclusion and summary

We have considered step scaling based on the gradient flow renormalized coupling, introducing a non-perturbative  $\mathcal{O}(a^2)$  improvement that removes, or at least greatly reduces, leading-order cut-off effects. This phenomenological improvement increases our control over the extrapolation to the infinite-volume continuum limit, as we demonstrated first for the case of SU(3) gauge theory with  $N_f = 4$  massless staggered fermions. Turning to  $N_f = 12$ , we found that the continuum limit was well defined and predicted an infrared fixed point even without improvement. Applying our proposed improvement reinforced this conclusion by removing all observable  $\mathcal{O}(a^2)$  effects. For the finite-volume gradient flow renormalization scheme defined by  $c = 0.2$ , we find the continuum conformal fixed point to be located at  $g_\star^2 = 6.18(20)$ .

The 12-flavor system has been under investigation for some time, and other groups have studied its step scaling function [42, 7, 8, 40]. However, this work is the first to observe an IRFP in the infinite-volume continuum limit. There are likely several factors contributing to this progress. While we did not invest more computer time than other groups, we have employed a well-designed lattice action. The adjoint plaquette term in our gauge action moves us farther away from a well-known spurious fixed point, while nHYP smearing allows us to simulate at relatively strong couplings. The gradient flow coupling itself appears to be a significant improvement over other schemes,<sup>3</sup> and our non-perturbative improvement also contributes to obtaining more reliable continuum extrapolations.

Our non-perturbative improvement is general and easy to use in other systems. It does not rely on the lattice action or fermion discretization, though we suspect that the improvement may not be effective if there are  $\mathcal{O}(a)$  artifacts, e.g. for unimproved Wilson fermions. Since  $\mathcal{O}(a)$ -improved

---

<sup>3</sup> C.-J. D. Lin has told us about dramatic improvements in auto-correlations when using the gradient flow coupling compared to the twisted Polyakov loop coupling of Ref. [42].

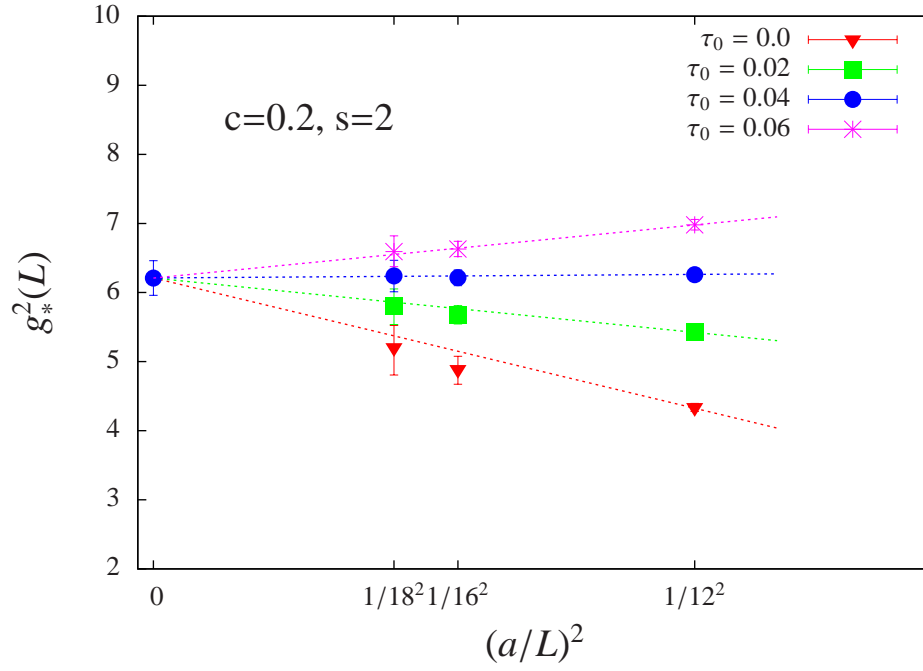


Figure 5.4: Continuum extrapolations of the 12-flavor finite volume IRFP  $g_*^2(L)$ , with several different  $t$ -shift coefficients  $\tau_0$  for fixed scale change  $s = 2$ . The dotted lines are a joint linear fit constrained to have the same  $(a/L)^2 = 0$  intercept, which gives  $g_*^2 = 6.21(25)$ .

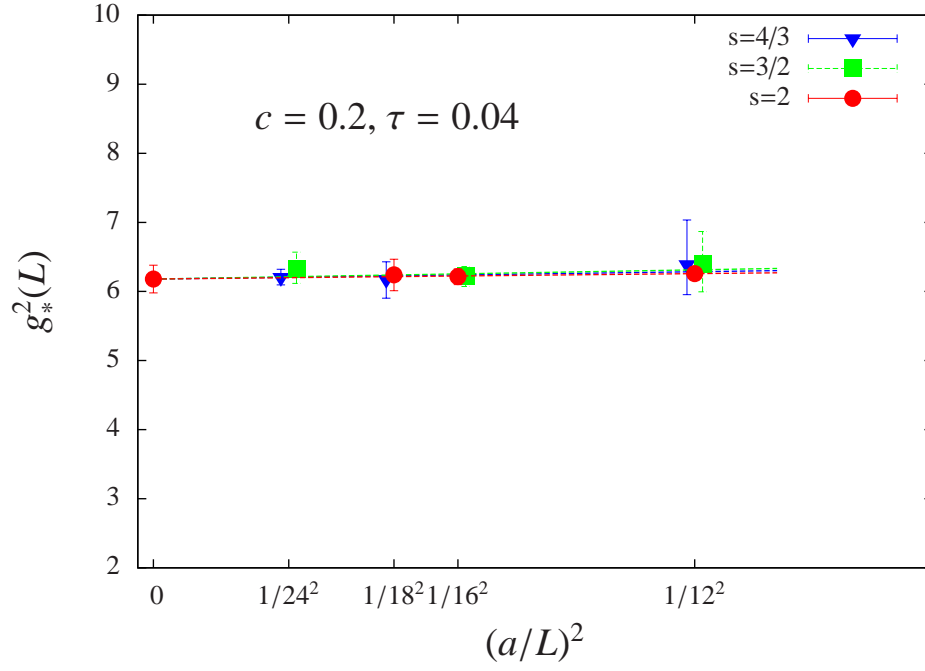


Figure 5.5: Continuum extrapolations of the 12-flavor finite volume IRFP  $g_*^2(L)$ , with several different scale changes for the near-optimal improvement coefficient  $\tau_{\text{opt}} \approx 0.04$ . The  $s = 4/3$  and  $3/2$  data points are horizontally displaced for greater clarity. The dashed lines are a joint linear fit constrained to have the same  $(a/L)^2 = 0$  intercept, which gives  $g_*^2 = 6.18(20)$ .



lattice actions are standard, this does not appear to be a practical limitation. We look forward to seeing our proposal applied both to QCD and to other conformal or near-conformal systems.

## **5.8 Wilson Flow MCRG Results**

## Chapter 6

### Wilson Flow MCRG

#### 6.1 MCRG Results

The renormalization group has been used to study the  $SU(3)$   $N_f = 12$  system already [cite anna]. These results show that the theory is clearly conformal. The action used in these simulations is ... As part of a greater effort to study this system further we changed our action to reach stronger coupling. In this section I will present our results using MCRG with the changed action.

##### 6.1.1 The Simulation

To achieve stronger coupling we use a different lattice action. This action has [details about action]

#### 6.2 Wilson Flow Results

For the past several years many lattice groups have been involved in studying strongly-coupled near-conformal gauge–fermion systems. Some of these models may be candidates for new physics beyond the standard model, while others are simply interesting non-perturbative quantum field theories. Because the dynamics of these lattice systems are unfamiliar, it is important to study them with several complementary techniques. Not only does this allow consistency checks, it can also provide information about the most efficient and reliable methods to investigate near-conformal lattice theories.

Monte Carlo Renormalization Group (MCRG) two-lattice matching is one of several analysis tools that we are using to investigate SU(3) gauge theories with many massless fermion flavors. This technique predicts the step-scaling function  $s_b$  in the bare parameter space. In a previous work [49] we proposed an improved MCRG method that exploits the Wilson flow to obtain a bare step-scaling function that corresponds to a unique discrete  $\beta$  function. We briefly review our Wilson-flow-optimized MCRG (WMCRG) procedure in Sections 6.3–6.4. It is important to note that we are investigating a potential infrared fixed point (IRFP) where the coupling is irrelevant: its running slows and eventually stops. This is challenging to distinguish from a near-conformal system where the gauge coupling runs slowly but does not flow to an IRFP. The observation of a backward flow that survives extrapolation to the infinite-volume limit could provide a clean signal. In Section 6.5 we report WMCRG results for SU(3) gauge theory with  $N_f = 12$  flavors of massless fermions in the fundamental representation.

This 12-flavor model has been studied by many groups, including Refs. [8, 20, 22, 5, 34, 19, 18, 41, 42, 4, 23, 24, 40, 16, 2, 36, 37, 17]. Using new ensembles of 12-flavor gauge configurations generated with exactly massless fermions, our improved WMCRG technique predicts a conformal IRFP where the step-scaling function vanishes. As with every method, it is essential to study the systematic effects. For WMCRG the most important systematic effects are due to the finite volume and limited number of blocking steps. While we are not able to carry out a rigorous infinite-volume extrapolation, the observed zero of the bare step-scaling function is present for all investigated lattice volumes and renormalization schemes, and agrees with the earlier MCRG results of Ref. [34]. The results of our complementary  $N_f = 12$  investigations of finite-temperature phase transitions [52, 36], the Dirac eigenmode number [16, 17], and finite-size scaling [37] are also consistent with the existence of an infrared fixed point and IR conformality.

### 6.3 Monte Carlo Renormalization Group

MCRG techniques probe lattice field theories by applying RG blocking transformations that integrate out high-momentum (short-distance) modes, moving the system in the infinite-

dimensional space of lattice-action couplings. In an IR-conformal system on the  $m = 0$  critical surface, a renormalized trajectory runs from the perturbative gaussian FP (where the gauge coupling  $\beta$  is a relevant operator) to the IRFP (where  $\beta$  is irrelevant). Because the locations of these fixed points in the action-space depend on the renormalization scheme, each scheme corresponds to a different renormalized trajectory. The RG flow produced by the blocking steps moves the system towards and along the renormalized trajectory, from the perturbative FP to the infrared fixed point. At stronger couplings, where we would naïvely expect backward flow, there might be no ultraviolet FP to drive the RG flow along a renormalized trajectory. Except in the immediate vicinity of the IRFP, every method that attempts to determine the strong-coupling flow of the gauge coupling (including MCRG two-lattice matching) might then become meaningless.

We determine the bare step-scaling function  $s_b(\beta_1)$  by matching the lattice actions  $S(\beta_1, n_b)$  and  $S(\beta_2, n_{b-1})$  for systems with bare couplings  $\{\beta_1, \beta_2\}$  after  $\{n_b, n_{b-1}\}$  blocking steps:  $s_b(\beta_1) \equiv \lim_{n_b \rightarrow \infty} \beta_1 - \beta_2$  [49]. When the lattice actions are identical, all observables are identical. We use the plaquette, the three six-link loops and a planar eight-link loop to perform this matching. Using short-distance gauge observables allows us to carry out more blocking steps, down to small  $2^4$  or  $3^4$  lattices. We minimize finite-volume effects by comparing observables measured on the same blocked volume [34]. We perform the matching independently for each observable, fitting the data as a cubic function of  $\beta$  to smoothly interpolate between investigated values of the gauge coupling.

Our finite lattices only allow a few blocking steps, so we must optimize the procedure to reach the renormalized trajectory in as few steps as possible. In practice, we optimize by tuning some parameter so that consecutive RG blocking steps yield the same  $\beta_1 - \beta_2$ , which we identify as  $s_b(\beta_1)$ . Traditional optimization tunes the RG blocking transformation at each coupling separately, resulting in a different renormalization scheme at each bare coupling  $\beta_1$ : the  $s_b$  we obtain is a composite of many different discrete  $\beta$  functions. The Wilson flow provides a parameter that we can tune without changing the scheme.

## 6.4 Wilson-flow-optimized MCRG

The Wilson flow is a continuous smearing transformation [46] that removes UV fluctuations without changing the lattice scale, as shown in Fig. 6.1. In perturbation theory it is related to the  $\overline{\text{MS}}$  running coupling [43], and can be used to compute a renormalized step-scaling function [26, 27].

In this work we use the Wilson flow to optimize MCRG two-lattice matching with a fixed RG blocking transformation (renormalization scheme). The Wilson flow continuously moves the system on a surface of constant lattice scale in the infinite-dimensional space of lattice-action couplings. We tune the flow time to bring the system as close as possible to the renormalized trajectory. After running the optimal amount of Wilson flow on the unblocked lattices, we then carry out the MCRG two-lattice matching. Because the renormalization scheme is fixed, we obtain a bare step-scaling function that corresponds to a unique discrete  $\beta$  function.

## 6.5 Results for 12 Flavors

Our WMCRG results for the 12-flavor system are obtained on gauge configurations generated with exactly massless fermions. Our lattice action uses nHYP-smeared staggered fermions as described in Ref. [18], and to run with  $m = 0$  we employ anti-periodic boundary conditions in all four directions. All of our analyses are carried out at couplings weak enough to avoid the unusual strong-coupling “ $\mathcal{S}^4$ ” phase discussed by Refs. [18, 36].

We perform three-lattice matching with volumes  $6^4\text{--}12^4\text{--}24^4$  and  $8^4\text{--}16^4\text{--}32^4$ . Three-lattice matching is based on two sequential two-lattice matching steps, to minimize finite-volume effects [34]. Both two-lattice matching steps are carried out on the same final volume  $V_f$ . We denote the number of blocking steps on the largest volume by  $n_b$ , and tune the length of the initial Wilson flow by requiring that the last two blocking steps predict the same step-scaling function. Using the  $8^4\text{--}16^4\text{--}32^4$  data we determine the bare step-scaling function for  $n_b = 3$  and  $V_f = 4^4$  as well as  $n_b = 4$  and  $V_f = 2^4$ , while the  $6^4\text{--}12^4\text{--}24^4$  data set is blocked to a final volume  $V_f = 3^4$  ( $n_b = 3$ ). This allows us to explore the effects of both the final volume and the number of blocking

steps. We investigate three renormalization schemes by changing the HYP smearing parameters in our blocking transformation [49]: scheme 1 uses smearing parameters (0.6, 0.2, 0.2), scheme 2 uses (0.6, 0.3, 0.2) and scheme 3 uses (0.65, 0.3, 0.2).

Figs. 6.2, 6.3 and 6.4 present representative results for 12 flavors. All of the bare step-scaling functions clearly show  $s_b = 0$ , signalling an infrared fixed point, for every  $n_b$ ,  $V_f$  and renormalization scheme. Appropriately for an IR-conformal system, the location of the fixed point is scheme dependent. We observe that the fixed point moves to stronger coupling as the HYP smearing parameters in the RG blocking transformation increase.

When we block our  $8^4$ ,  $16^4$  and  $32^4$  lattices down to a final volume  $V_f = 2^4$  (corresponding to  $n_b = 4$ ), the observables become very noisy, making matching more difficult. The problem grows worse as the HYP smearing parameters increase, and our current statistics do not allow reliable three-lattice matching for  $V_f = 2^4$  in schemes 2 and 3. To resolve this issue, we are accumulating more statistics in existing  $32^4$  runs, and generating additional  $32^4$  ensembles at more values of the gauge coupling  $\beta_F$ . These additional data will also improve our results for scheme 1, which we show in Fig. 6.4. Different volumes and  $n_b$  do not produce identical results in scheme 1, suggesting that the corresponding systematic effects are still non-negligible. We can estimate finite-volume effects by comparing  $n_b = 3$  with  $V_f = 3^4$  and  $V_f = 4^4$ . Systematic effects due to  $n_b$  can be estimated from  $n_b = 4$  and  $V_f = 2^4$ , but this is difficult due to the noise in the  $2^4$  data. Even treating the spread in the results shown in Fig. 6.4 as a systematic uncertainty, we still obtain a clear zero in the bare step-scaling function, indicating an IR fixed point.

## 6.6 Conclusion

In this proceedings we have shown how the Wilson-flow-optimized MCRG two-lattice matching procedure proposed in Ref. [49] improves upon traditional lattice renormalization group techniques. By optimizing the flow time for a fixed RG blocking transformation, WMCRG predicts a bare step-scaling function  $s_b$  that corresponds to a unique discrete  $\beta$  function. Applying WMCRG to new 12-flavor ensembles generated with exactly massless fermions, we observe an infrared fixed

point in  $s_b$ . The fixed point is present for all investigated lattice volumes, number of blocking steps and renormalization schemes, even after accounting for systematic effects indicated by Fig. 6.4. This result reinforces the IR-conformal interpretation of our complementary  $N_f = 12$  studies of phase transitions [52, 36], the Dirac eigenmode number [16, 17], and finite-size scaling [37].

## 6.7 Wilson Flow MCRG Results

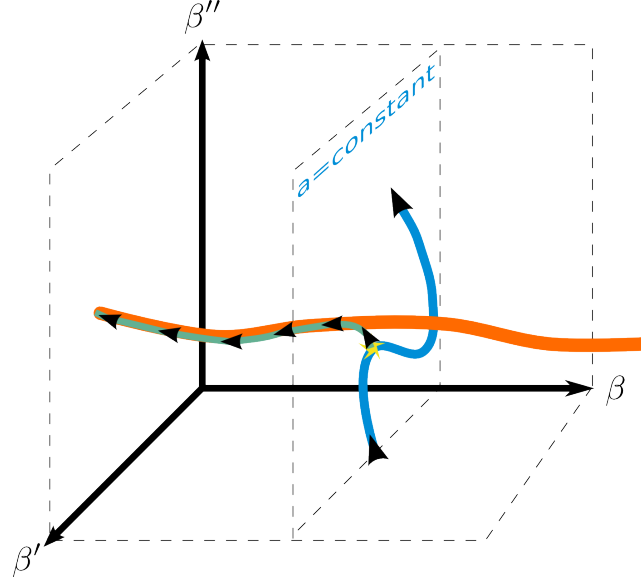


Figure 6.1: The Wilson flow (blue) moves systems on a surface of constant lattice scale  $a$  (normal to the orange renormalized trajectory) in the infinite-dimensional coupling space. Wilson-flow-optimized MCRG tunes the flow time to bring the system close to the renormalized trajectory (yellow star), so that MCRG blocking (green) quickly reaches the renormalized trajectory.

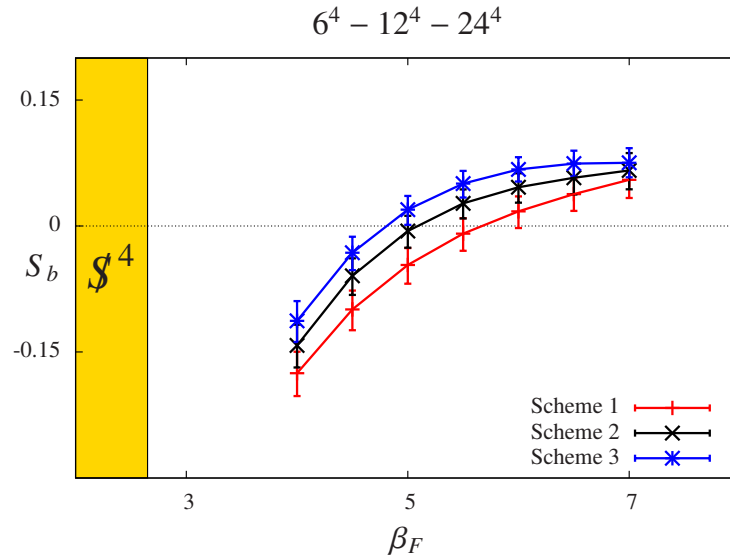


Figure 6.2: The bare step-scaling function  $s_b$  predicted by three-lattice matching with  $6^4$ ,  $12^4$  and  $24^4$  lattices blocked down to  $3^4$ , comparing three different renormalization schemes. The error bars come from the standard deviation of predictions using the different observables discussed in Section 6.3.



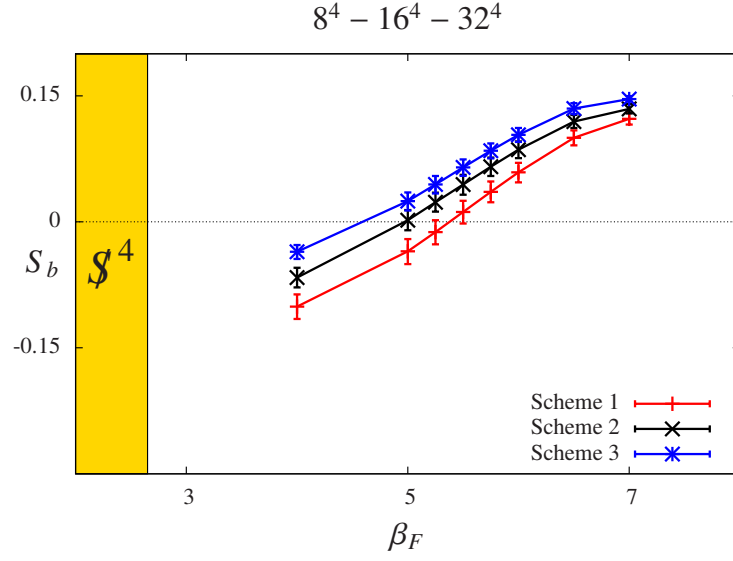


Figure 6.3: As in Fig. 6.2, the bare step-scaling function  $s_b$  for three different renormalization schemes from three-lattice matching, now using  $8^4$ ,  $16^4$  and  $32^4$  lattices blocked down to  $4^4$ .

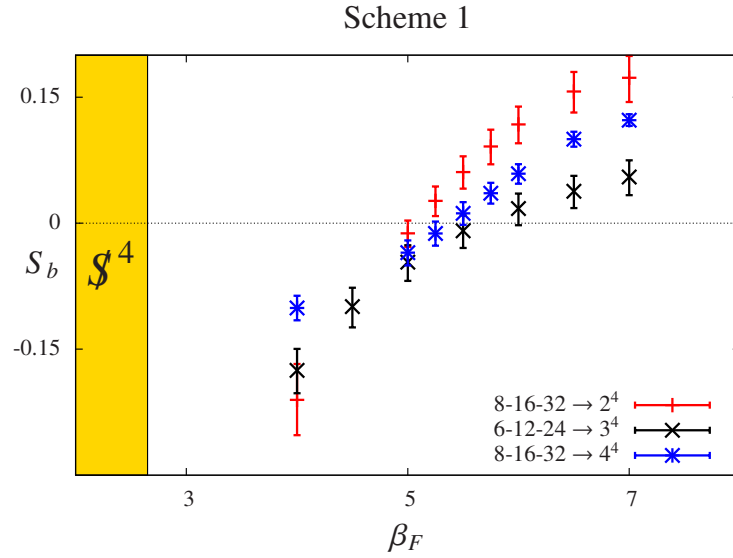


Figure 6.4: The bare step-scaling function  $s_b$  for scheme 1, comparing three-lattice matching using different volumes:  $6^4$ ,  $12^4$  and  $24^4$  lattices blocked down to  $3^4$  (black  $\times$ s) as well as  $8^4$ ,  $16^4$  and  $32^4$  lattices blocked down to  $4^4$  (blue bursts) and  $2^4$  (red crosses).

## Bibliography

- [1] Yasumichi Aoki, Tatsumi Aoyama, Masafumi Kurachi, Toshihide Maskawa, Kohtaroh Miura, Kei-ichi Nagai, Hiroshi Ohki, Enrico Rinaldi, Akihiro Shibata, Koichi Yamawaki, and Takeshi Yamazaki. Light composite scalar in eight-flavor QCD on the lattice. 2014.
- [2] Yasumichi Aoki, Tatsumi Aoyama, Masafumi Kurachi, Toshihide Maskawa, Kei-ichi Nagai, Hiroshi Ohki, Enrico Rinaldi, Akihiro Shibata, Koichi Yamawaki, and Takeshi Yamazaki. 2013.
- [3] Yasumichi Aoki, Tatsumi Aoyama, Masafumi Kurachi, Toshihide Maskawa, Kei-ichi Nagai, Hiroshi Ohki, Enrico Rinaldi, Akihiro Shibata, Koichi Yamawaki, and Takeshi Yamazaki. Light composite scalar in twelve-flavor QCD on the lattice. Phys. Rev. Lett., 111:162001, 2013.
- [4] Yasumichi Aoki, Tatsumi Aoyama, Masafumi Kurachi, Toshihide Maskawa, Kei-ichi Nagai, Hiroshi Ohki, Akihiro Shibata, Koichi Yamawaki, and Takeshi Yamazaki. Phys. Rev., D86:054506, 2012.
- [5] T. Appelquist, G. T. Fleming, M. F. Lin, E. T. Neil, and D. Schaich. Phys. Rev., D84:054501, 2011.
- [6] Thomas Appelquist, Richard Brower, Simon Catterall, George Fleming, Joel Giedt, Anna Hasenfratz, Julius Kuti, Ethan Neil, and David Schaich. Lattice Gauge Theories at the Energy Frontier. 2013.
- [7] Thomas Appelquist, George T. Fleming, and Ethan T. Neil. Lattice study of the conformal window in QCD-like theories. Phys. Rev. Lett., 100:171607, 2008.
- [8] Thomas Appelquist, George T. Fleming, and Ethan T. Neil. Phys. Rev., D79:076010, 2009.
- [9] Janos Balog, Ferenc Niedermayer, and Peter Weisz. Logarithmic corrections to  $O(a^{**2})$  lattice artifacts. Phys. Lett., B676:188–192, 2009.
- [10] Janos Balog, Ferenc Niedermayer, and Peter Weisz. The Puzzle of apparent linear lattice artifacts in the 2d non-linear sigma-model and Symanzik’s solution. Nucl. Phys., B824:563–615, 2010.
- [11] Tom Banks and A. Zaks. On the Phase Structure of Vector-Like Gauge Theories with Massless Fermions. Nucl. Phys., B196:189, 1982.

- [12] Szabolcs Borsanyi, Stephan Durr, Zoltan Fodor, Christian Hoelbling, Sandor D. Katz, S. Krieg, T. Kurth, L. Lellouch, T. Lippert, C. McNeile, and K. K. Szabo. JHEP, 1209:010, 2012.
- [13] William E. Caswell. Asymptotic Behavior of Nonabelian Gauge Theories to Two Loop Order. Phys. Rev. Lett., 33:244, 1974.
- [14] Anqi Cheng, Anna Hasenfratz, Yuzhi Liu, Gregory Petropoulos, and David Schaich. Finite size scaling of conformal theories in the presence of a near-marginal operator. 2013.
- [15] Anqi Cheng, Anna Hasenfratz, Yuzhi Liu, Gregory Petropoulos, and David Schaich. Step scaling studies using the gradient flow running coupling. 2014, in preparation.
- [16] Anqi Cheng, Anna Hasenfratz, Gregory Petropoulos, and David Schaich. JHEP, 1307:061, 2013.
- [17] Anqi Cheng, Anna Hasenfratz, Gregory Petropoulos, and David Schaich. PoS, LATTICE 2013:088, 2013.
- [18] Anqi Cheng, Anna Hasenfratz, and David Schaich. Phys. Rev., D85:094509, 2012.
- [19] Thomas DeGrand. Phys. Rev., D84:116901, 2011.
- [20] A. Deuzeman, M. P. Lombardo, and E. Pallante. Phys. Rev., D82:074503, 2010.
- [21] Albert Deuzeman, Maria Paola Lombardo, Tiago Nunes da Silva, and Elisabetta Pallante. 2012.
- [22] Zoltan Fodor, Kieran Holland, Julius Kuti, Daniel Nogradi, and Chris Schroeder. Phys. Lett., B703:348–358, 2011.
- [23] Zoltan Fodor, Kieran Holland, Julius Kuti, Daniel Nogradi, Chris Schroeder, and Chik Him Wong. PoS, Lattice 2012:025, 2012.
- [24] Zoltan Fodor, Kieran Holland, Julius Kuti, Daniel Nogradi, Chris Schroeder, and Chik Him Wong. 2012.
- [25] Zoltan Fodor, Kieran Holland, Julius Kuti, Daniel Nogradi, Chris Schroeder, and Chik Him Wong. Can the nearly conformal sextet gauge model hide the Higgs impostor? Phys. Lett., B718:657–666, 2012.
- [26] Zoltan Fodor, Kieran Holland, Julius Kuti, Daniel Nogradi, and Chik Him Wong. 2012.
- [27] Zoltan Fodor, Kieran Holland, Julius Kuti, Daniel Nogradi, and Chik Him Wong. PoS, Lattice 2012:050, 2012.
- [28] Zoltan Fodor, Kieran Holland, Julius Kuti, Daniel Nogradi, and Chik Him Wong. Can a light Higgs impostor hide in composite gauge models? PoS, LATTICE 2013:062, 2014.
- [29] Patrick Fritzsche and Alberto Ramos. The gradient flow coupling in the Schrödinger Functional. JHEP, 1310:008, 2013.
- [30] Joel Giedt. PoS, Lattice 2012:006, 2012.

- [31] Joel Giedt. Lattice gauge theory and physics beyond the standard model. PoS, Lattice 2012:006, 2012.
- [32] Anna Hasenfratz. Conformal or Walking? Monte Carlo renormalization group studies of SU(3) gauge models with fundamental fermions. Phys. Rev., D82:014506, 2010.
- [33] Anna Hasenfratz. PoS, Lattice 2011:065, 2011.
- [34] Anna Hasenfratz. Phys. Rev. Lett., 108:061601, 2012.
- [35] Anna Hasenfratz, Anqi Cheng, Gregory Petropoulos, and David Schaich. PoS, Lattice 2012:034, 2012.
- [36] Anna Hasenfratz, Anqi Cheng, Gregory Petropoulos, and David Schaich. 2013.
- [37] Anna Hasenfratz, Anqi Cheng, Gregory Petropoulos, and David Schaich. PoS, LATTICE 2013:075, 2013.
- [38] Anna Hasenfratz, Roland Hoffmann, and Stefan Schaefer. Hypercubic smeared links for dynamical fermions. JHEP, 0705:029, 2007.
- [39] Anna Hasenfratz and Francesco Knechtli. Flavor symmetry and the static potential with hypercubic blocking. Phys. Rev., D64:034504, 2001.
- [40] Etsuko Itou. PTEP, 2013:083B01, 2013.
- [41] Xiao-Yong Jin and Robert D. Mawhinney. PoS, Lattice 2011:066, 2012.
- [42] C.-J. David Lin, Kenji Ogawa, Hiroshi Ohki, and Eigo Shintani. JHEP, 1208:096, 2012.
- [43] Martin Luscher. JHEP, 1008:071, 2010.
- [44] Martin Luscher. Trivializing maps, the Wilson flow and the HMC algorithm. Commun. Math. Phys., 293:899–919, 2010.
- [45] Shinya Matsuzaki and Koichi Yamawaki. Holographic techni-dilaton at 125 GeV. Phys. Rev., D86:115004, 2012.
- [46] R. Narayanan and H. Neuberger. JHEP, 0603:064, 2006.
- [47] Ethan T. Neil. Exploring Models for New Physics on the Lattice. PoS, Lattice 2011:009, 2011.
- [48] Paula Perez-Rubio and Stefan Sint. Non-perturbative running of the coupling from four flavour lattice QCD with staggered quarks. PoS, Lattice 2010:236, 2010.
- [49] Gregory Petropoulos, Anqi Cheng, Anna Hasenfratz, and David Schaich. PoS, Lattice 2012:051, 2012.
- [50] Gregory Petropoulos, Anqi Cheng, Anna Hasenfratz, and David Schaich. Improved Lattice Renormalization Group Techniques. PoS, LATTICE 2013:079, 2013.
- [51] Thomas A. Ryttov and Robert Shrock. Phys.Rev., D86:085005, 2012.
- [52] David Schaich, Anqi Cheng, Anna Hasenfratz, and Gregory Petropoulos. PoS, Lattice 2012:028, 2012.

- [53] Rainer Sommer. Scale setting in lattice QCD. PoS, LATTICE 2013:015, 2014.
- [54] Fatih Tekin, Rainer Sommer, and Ulli Wolff. The Running coupling of QCD with four flavors. Nucl. Phys., B840:114–128, 2010.